Machine Learning-Based Quantitative Prediction of Hepatic Steatosis Using Ultrasound Signal Attenuation: A Validation Study with MRI-PDFF

Seong-Cheol Kwon and Seung-Man Yu *

Posted Date: 17 March 2026

doi: 10.20944/preprints202603.1260.v1

Keywords: fatty liver; MRI DIXON; ultrasonography; principal component analysis; attenuation coefficient; noninvasive assessment

 doi:10.20944/preprints202603.1260.v1

Article

Machine Learning-Based Quantitative Prediction of Hepatic Steatosis Using Ultrasound Signal Attenuation: A Validation Study with MRI-PDFF

Seong-Cheol Kwon [1,2] and Seung-Man Yu [2,*]

[1] Department of Radiology, Won Kwang University Hospital, Iksan 54538, Republic of Korea

[2] Department of Radiological Science, College of Medical Science, Jeonju University, Jeonju 55069, Republic of Korea

* Correspondence: ysm9993@jj.ac.kr; Tel.: +82 010-2902-1786

Abstract

Background/Objectives: This study aimed to develop and evaluate a prediction model for fatty liver (hepatic steatosis) using ultrasound-derived quantitative variables, with MRI DIXON-based fat fraction (MRI-FF) as the reference standard. **Methods:** Twenty-seven participants with above-normal BMI underwent ultrasound and MRI examinations concurrently. Ultrasound images of the liver, kidney, and spleen were acquired at dynamic range (DR) settings of 100, 150, and 200. Quantitative variables (signal intensity, linear slope, exponential attenuation coefficient, and R^2) were extracted using ImageJ. Key variables were selected via principal component analysis (PCA) and orthogonal partial least squares discriminant analysis (OPLS-DA) with VIP scores ≥1.25. A support vector machine (SVM) model was constructed using training (n=21) and validation (n=6) datasets. **Results:** PCA and OPLS-DA revealed that the liver-to-kidney attenuation ratio, liver attenuation R^2 (DR200), and linear slope R^2 (DR200) correlated most strongly with MRI-FF (r=0.814, 0.753, 0.724; all $p < 0.001$). Attenuation variables were significantly higher in fatty liver groups across all MRI-FF thresholds. The SVM model demonstrated excellent predictive performance (RMSE=2.1997, r=0.82, $p < 0.001$). **Conclusions:** Ultrasound-derived signal attenuation characteristics correlate strongly with MRI-FF, enabling accurate quantitative assessment of hepatic steatosis through machine learning. This noninvasive, cost-effective approach shows significant potential for screening and longitudinal monitoring of fatty liver disease.

Keywords: fatty liver; MRI DIXON; ultrasonography; principal component analysis; attenuation coefficient; noninvasive assessment

1. Introduction

Fatty liver is a condition in which there is an excessive accumulation of triglycerides in hepatocytes [1], which is an important disease to manage without symptoms at the beginning but can progress to non-alcoholic steatohepatitis (NASH), fibrosis, cirrhosis, and even hepatocellular carcinoma over time [2].This progression pathway leads from simple lipid deposition to chronic inflammation, fibrosis, and changes in tissue structure. Without early diagnosis and continuous follow-up management, the prognosis can deteriorate rapidly. This serves as the basis for considering fatty liver disease not merely a liver disorder but a central axis of metabolic disease [3]. Therefore, the need for early diagnosis and quantitative monitoring of fatty liver disease is increasingly emphasized [4].

The primary methods for diagnosing fatty liver in clinical practice are currently classified as ultrasonography, computed tomography (CT), and magnetic resonance imaging (MRI) [5]. Among these, abdominal ultrasonography is the most widely used in medical institutions due to its relatively low cost, non-invasive nature, and ability to provide real-time imaging [6]. However, ultrasound-

 doi:10.20944/preprints202603.1260.v1

based fatty liver diagnosis heavily relies on the examiner's skill and experience. There is also the issue that the brightness (echogenicity) of the liver parenchyma and the liver-to-kidney contrast ratio can vary depending on equipment settings (such as Dynamic Range and Gain) [7]. Indeed, while increased liver brightness in ultrasound images is interpreted as an indicator of fat deposition, signal contrast can vary depending on operator manipulation even in the same patient. This makes quantitative evaluation difficult, necessitating reliance on subjective judgment [8].

In ultrasound diagnosis, the cortex or medulla of the kidney is commonly used as a reference standard. If the brightness of the liver parenchyma is relatively brighter than that of the kidney, it is diagnosed as fatty liver [9]. However, this method can be affected by the dynamic range (DR) settings, which artificially alter the image contrast, and the attenuation characteristics of ultrasound waves with depth also influence signal interpretation. [10]. This examiner's dependency and sensitivity to imaging parameters have been major factors complicating the quantitative assessment of fatty liver using ultrasound [11]. Nevertheless, recent studies have consistently attempted to quantitatively analyze the physical characteristics of ultrasound signals [12]. Studies quantifying liver brightness (mean intensity), standard deviation of reflectivity, and attenuation coefficients with depth have begun to emerge [13]. Previously, efforts focused on compensating for signal attenuation with depth using the Time Gain Compensation (TGC) function of ultrasound equipment to standardize image quality [14]. However, this compensation method fails to reflect the signal attenuation characteristics specific to fat content itself [15]. This study aims to quantify the attenuation characteristics of ultrasound signals caused by fat deposition itself and utilize this as an objective indicator for fatty liver diagnosis. Unlike the existing subjective diagnosis based on 'comparison with the kidney,' this approach can function as a new imaging-based biomarker that directly quantifies the physical attenuation characteristics within a single organ.

Meanwhile, principal component analysis is employed as a statistical method to identify variables exhibiting differences between groups across various variables [16]. Principal Component Analysis (PCA) is a dimensionality reduction technique that analyzes correlations among multiple variables to explain the inherent variance within the data, deriving a small number of principal components through combinations of these variables [17]. PCA simplifies complex, high-dimensional data to identify key patterns within the data structure and enables the identification of the most important variables based on the variance explained by each principal component [18]. This analytical technique allows for the quantitative analysis of changes in data patterns according to the severity and pathological state of fatty liver disease. PCA summarizes the correlation structure among multidimensional variables and maximizes explanatory power using only the principal components, thereby simplifying predictive models and enhancing interpretability [19].

MRI is recognized as the most accurate method for diagnosing and quantitatively assessing fatty liver disease [20], and MRI fat fraction (MRI-FF) based on Dixon techniques is considered the gold standard for noninvasive, quantitative measurement of fat content [21]. Indeed, MRI-FF values of 5% or higher are considered indicative of fatty liver disease [22], and this criterion is known to show a strong correlation with histopathological findings [23]. However, to date, these imaging-based quantitative models remain in the early research stage [24], and studies systematically elucidating the relationship between the physical signal characteristics of ultrasound images and fat content, using MRI-FF as a reference, differ from existing research (e.g., comparisons by DR conditions, utilization of long-term ratio variables, etc.) [25]. Therefore, if MRI-FF can be predicted using quantitative variables extracted from ultrasound images, it could offer a cost-effective and highly accessible alternative method for diagnosing fatty liver disease. In other words, if MRI-level fat quantification is achievable using ultrasound alone, it could significantly reduce unnecessary MRI examinations and be utilized for early screening and follow-up monitoring, yielding substantial clinical and economic benefits. Traditional ultrasound-based diagnosis heavily relied on the subjective judgment of the operator, limiting reproducibility and quantitative assessment. However, by integrating AI-based machine learning techniques, it is expected that signal characteristics and patterns derived from ultrasound images can be quantitatively analyzed. Furthermore, through

 doi:10.20944/preprints202603.1260.v1

comparison and validation with the MRI-DIXON technique, a more objective and reliable fatty liver prediction model can be presented.

This study measures the echo signals and depth information of the liver, kidney, and spleen in ultrasound images under various DR conditions and to develop a machine learning-based model that predicts the presence of fatty liver disease based on MRI-FF criteria using image-based variables (mean, standard deviation, attenuation coefficient, contrast ratio, etc.) derived from these measurements. This study aims to confirm the feasibility of a machine learning-based prediction model that can predict fatty liver based on objective and reproducible quantitative indicators, independent of the subjective interpretation methods used in conventional ultrasound imaging.

2. Materials and Methods

This study was conducted with the approval of the Jeonju University Institutional Review Board (jjIRB-250529-HR-2023-1012). This study aimed to evaluate the consistency between ultrasound diagnostic results and MRI DIXON-based in-vivo liver fat content measurements obtained from the same healthy subjects with obesity indicators. It also sought to explore the feasibility of developing a prediction model based on quantitative variables derived from ultrasound images. Participants were recruited from the general healthy population with a Body Mass Index (BMI) exceeding the normal range. Data were collected from 29 subjects (16 males, 13 females) who underwent sequential acquisition of ultrasound images of the liver parenchyma and MRI DIXON examinations at the same subject level. Inclusion criteria were as follows:

1. Healthy individuals who understood the study purpose and procedures and voluntarily expressed willingness to participate;
2. Individuals with a BMI exceeding the normal range according to institutional health screening standards;
3. Individuals for whom both ultrasound imaging of the liver parenchyma and MRI DIXON examination were feasible.

2.1. Ultrasound Imaging Acquisition Method

As shown in (Figure 1), ultrasound examinations were performed on the liver, spleen, and kidney using a general-purpose ultrasound imaging diagnostic device (Samsung Medison H60) according to the abdominal acquisition protocol at the region where parenchymal vascular structures were minimally observed. Images of each organ were acquired under identical conditions without adjusting TGC, with DR set to 100, 150, and 200, respectively. Quantitative analysis of the acquired ultrasound images was performed using the 'ImageJ' program (National Institutes of Health, USA). The Region of Interest (ROI) was set parallel to the direction of the ultrasound beam propagation from the organ surface and positioned as straight as possible to the end of the organ parenchyma. Care was taken during ROI placement to exclude obvious ultrasound artifacts or non-parenchymal structures such as vessels, bile ducts, cysts, or calcifications. To maintain consistency in repeated measurements within the same subject, the ROI was placed at a similar depth and position for all three organs to ensure reproducibility of the analysis.

 doi:10.20944/preprints202603.1260.v1

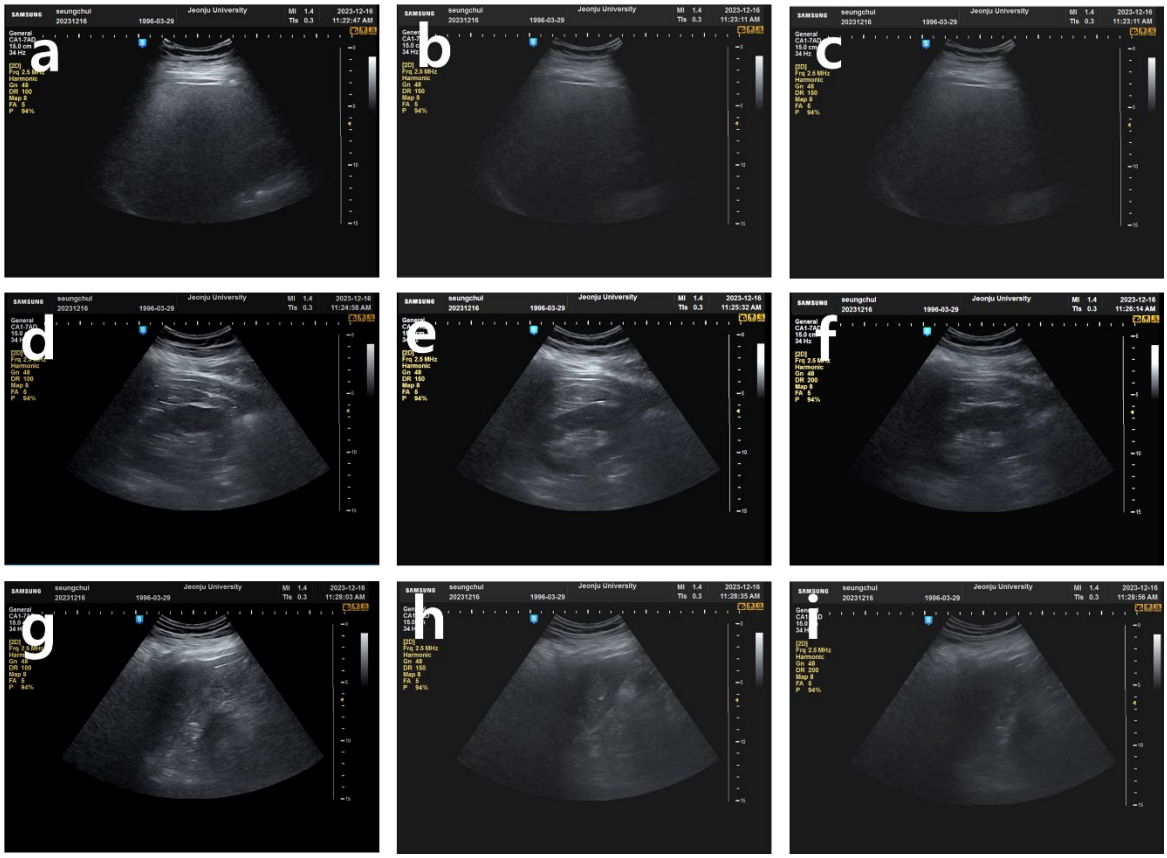

Figure 1. Ultrasound images of the liver, spleen, and kidney were obtained at regions with minimal intraparenchymal vascular structures using an abdominal imaging protocol. Each organ was scanned under identical conditions without TGC adjustment, with dynamic ranges (DR) set to 100, 150, and 200. Quantitative image analysis was performed using ImageJ software (National Institutes of Health, USA). For reference, the datasets were labeled as follows: a = DR 100 Liver, b = DR 150 Liver, c = DR 200 Liver; d = DR 100 Kidney, e = DR 150 Kidney, f = DR 200 Kidney; g= DR 100 Spleen, h = DR 150 Spleen, i = DR 200 Spleen.

The acquired ultrasound images were analyzed using the ImageJ program to perform Plot Profile on the ROI area. The resulting gray value data was categorized by each DR condition (e.g., values DR 100), and gray value change curves with respect to depth were plotted. First, a linear trendline was applied to calculate the regression equation and coefficient of determination (R^2). For the same data, an exponential trendline was applied to additionally derive the exponential function equation and R^2 value. This enabled a comparative analysis of the attenuation characteristics between the linear and exponential models for each DR condition.

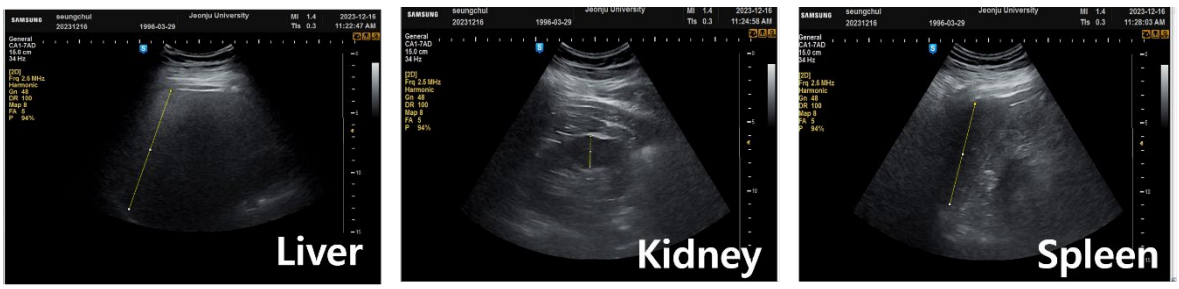

Figure 2. ROI placed parallel to ultrasound beam direction from organ surface; arranged linearly to distal parenchyma. Artifacts (vessels, ducts, cysts, calcifications) excluded. ROIs positioned at similar depth for consistency and reproducibility.

 doi:10.20944/preprints202603.1260.v1

2.2. MRI Dixon-based FF Numerical Acquisition and Group Classification Criteria

All subjects underwent ultrasound and MRI examinations consecutively on the same day. MRI examinations were performed using a Philips Elixion CX 3.0T system, with image acquisition employing a dStream Torso coil 32-channel (Flex Coverage Anterior coil and Posterior coil). The imaging protocol was based on the DIXON sequence with Repetition Time (TR): 5.7 ms, Echo Time (TE): 0.97 (TE1)/1.67 (TE2)/2.37 (TE3)/3.07 (TE4)/3.77 (TE5)/4.47 (TE6) ms. Slice thickness: 6 mm, number of slices: 67, slice gap: 0, acquisition voxel MPS (mm): 2.50/2.50/6.00, field of view (FOV): 310-400 (mm). As shown in (Figure 3), Water-only, In-phase (IP), Out-of-phase (OP), Fat-only, FF, and T2* images including the liver were acquired in the abdominal axial plane. Quantification of the Fat Fraction (FF) value was performed using a Philips dedicated workstation (PHILIPS-KL93MGI, Windows 10 Enterprise 2016 LTSB 64-bit). The section in the Dixon image, most anatomically similar to the measured liver parenchymal region in the ultrasound image was selected. As shown in (Figure 4), three circular ROIs with diameters of 15-20 mm were set at these locations. vessels, bile ducts, cysts, calcifications and other structures were excluded before measurements were calculated. The FF value was FF% = F/(W+F) *100 was calculated, and the average of the three points was recorded as the final FF value. The classification of hepatic fat accumulation severity referenced the FF criteria proposed in previous studies (normal liver: FF <5%, mild fatty liver: 5-10%, moderate fatty liver: 10-20%, severe fatty liver: >20%) [26]. However, in this study, grouping based on four criteria was concurrently applied to evaluate the model from multiple angles. Specifically, four classification systems were established and utilized for analysis: FF < 5% vs. ≥5%, FF <5% vs. ≥7%, FF <5% vs. ≥10%, and FF <5%vs. ≥15%.

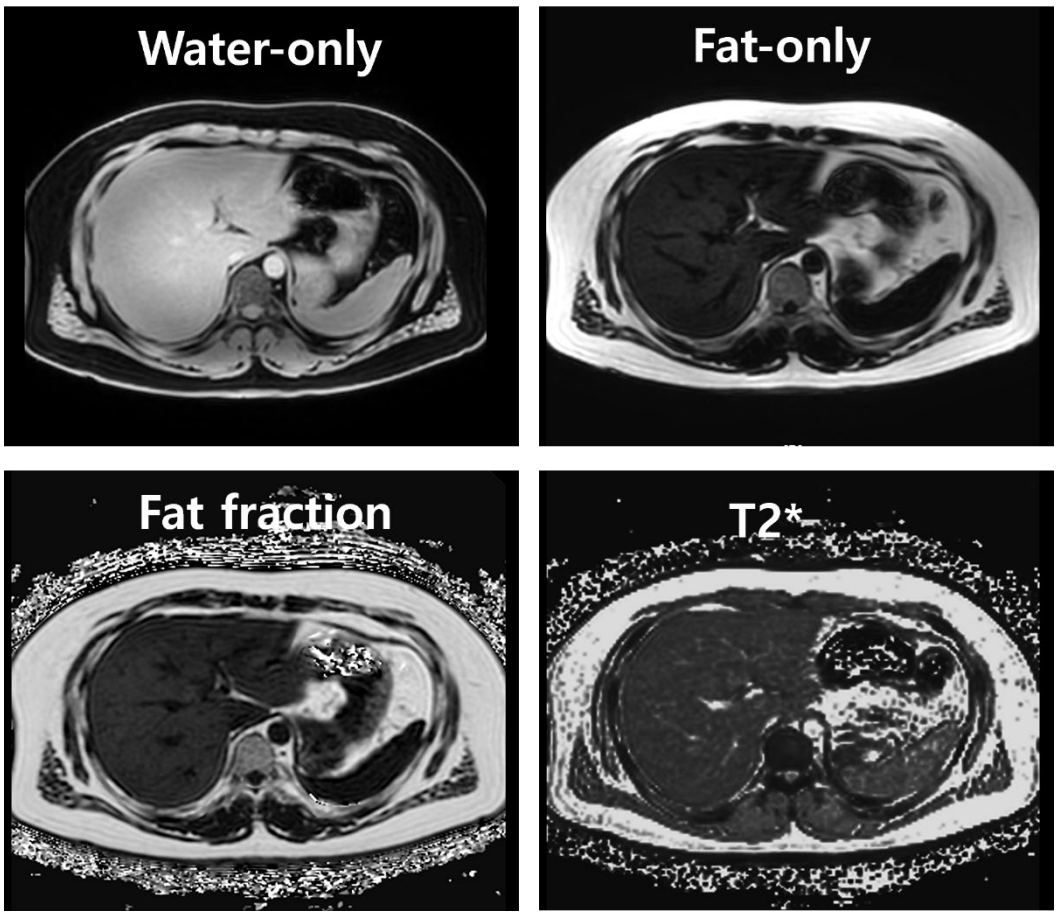

Figure 3. MRI performed on Philips Elition CX 3.0T with dStream Torso 32-channel coil (Flex Coverage Anterior and Posterior). DIXON sequence used (TR: 5.7 ms; TE: 0.97/0.7 ms; slice thickness: 6 mm; slices: 67; gap: 0; voxel size: 2.50 × 2.50 × 6.00 mm; FOV: 310–400 mm). Axial abdominal images acquired for liver in A = Water-only, B = Fat-only, C = FF, and D = T2 maps.

 doi:10.20944/preprints202603.1260.v1

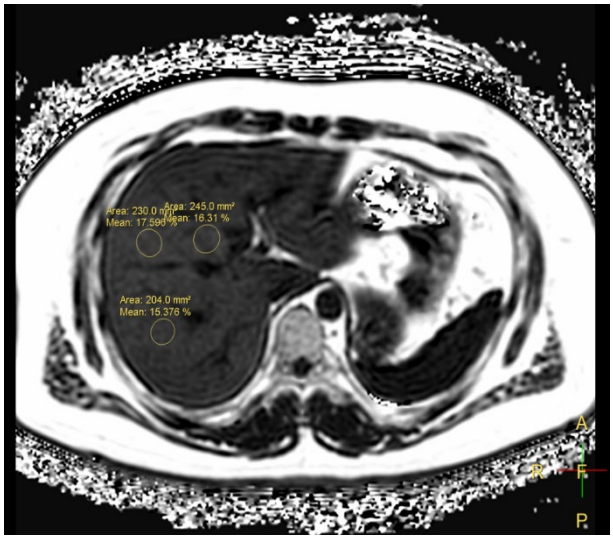

Figure 4. FF quantification performed using Philips workstation (PHILIPS-KL93MGI, Windows 10 Enterprise 2016 LTSB 64-bit). Circular ROIs (n=3) placed on Dixon images at anatomically matched liver sites corresponding to ultrasound measurements, avoiding vessels, bile ducts, cysts, and calcifications. FF value calculated automatically by the system; mean of three ROIs recorded as final FF positioned at similar depth for consistency and reproducibility.

2.3. Candidate Variable Design and Configuration

In this study, various candidate variables were designed based on signal data from the liver, spleen, and kidney obtained from ultrasound images. For each organ, images were acquired under DR 100, 150, and 200 conditions. Gray values within the ROI were extracted using ImageJ analysis and processed via linear regression and exponential regression analysis. First, the slope and coefficient of determination (R^2) of the linear trendline regression equation, and the decay coefficient (alpha) and coefficient of determination (R^2) of the exponential function equation were utilized as variables for each organ. For example, the slope values for the liver were named Liver Slope DR100, DR150, DR200, and the decay coefficients were named Liver Alpha DR100, DR150, DR200. Similarly, for the spleen and kidney, slope and alpha values, along with the R^2 values for each regression and exponential function equation, were set as independent variables. Second, we derived not only single indicators per maturity but also additional relative comparison and composite indicators. Specifically, these are as follows.

DR ratio variables obtained by dividing slope or alpha values under different DR conditions within the same maturity:

(e.g., Liver Slope Ratio = Slope_DR100/Slope_DR150, Slope_DR100/Slope_DR200, etc.) (1)

The DR-specific average values of slope and alpha within the same organ:

(e.g., Mean Liver Slope = (Slope_DR100+ Slope_DR150 + Slope_DR200)/3) (2)

Inter-organ relative ratio variables comparing slopes across different organs under the same DR condition:

(e.g., Slope_Liver100/Slope_Spleen100, Slope_Liver150/Slope_Kidney150, etc.) (3)

Cross-DR ratio variables comparing slopes between organs under different DR conditions:

(e.g., Slope_Liver100/ Slope_Spleen150) (4)

Standard Deviation (SD) and Relative Change Rate of slope or alpha values:

 doi:10.20944/preprints202603.1260.v1

(e.g., Slope SD_Liver = STDEV (Slope_DR100, Slope_DR150, Slope_DR200)) (5)

Slope change gradient to estimate slope variation patterns with DR changes:

(e.g., Slope_Gradient_Kidney = (Slope_DR200- Slope_DR150) - (Slope_DR150- Slope_DR100) (6)

Through this design process, we derived various composite indicators that go beyond simple single metrics, reflecting changes in DR conditions and comparisons across long-term periods. These candidate variables were subsequently selected as key explanatory variables through statistical analysis and principal component analysis (PCA) and were utilized as input variables for machine learning-based prediction models.

2.4. PCA, Statistical Analysis, and Key Variables

In this study, multivariate statistical techniques were applied to identify patterns in ultrasound-based candidate variables and evaluate their association with MRI-FF. First, principal component analysis (PCA) was performed using SIMCA software (version 14.1, Sartorius Stedim Data Analytics AB, Sweden). PCA was utilized to identify latent factors explaining the main variability in the data and to intuitively grasp the correlation structure between variables by projecting high-dimensional data onto a low-dimensional space based on the covariance structure between variables. PCA-X, partial least squares discriminant analysis (PLS-DA), and optimized partial least squares discriminant analysis (OPLS-DA) were applied stepwise for each group based on the MRI DIXON-FF criteria. These yielded results including score scatter plots, loading scatter plots, S-plots, and Variable Importance in Projection (VIP) scores. Variables with a VIP score of 1.0 or higher were prioritized as primary candidate variables. In the first PCA analysis, these were categorized into three intervals: VIP Score ≥ 1.0, 1.5, and 2.0. The selected variables underwent secondary analysis using the same methodology to re-extract those meeting a VIP score ≥ 1.0. Key variables were then selected by dividing them into two intervals: VIP Score ≥ 1.0 and ≥ 1.25. This process established stable and consistent key variables for each MRI FF group. The final criterion of VIP Score ≥ 1.25 was set for the following reasons. In the initial PCA analysis, variables selected based on VIP ≥ 1.0 were excessively numerous (over 100 per MRI-FF group: <5% vs ≥5%, ≥7%, ≥10%, ≥15%), which could increase model complexity and heighten the risk of overfitting. Therefore, the secondary analysis aimed to select only those variables that consistently maintained high VIP scores across multiple MRI-FF threshold conditions. This approach seeks to build a clinically interpretable and practical model by minimizing the number of variables while maintaining predictive performance. Subsequent statistical analyses were performed using SPSS software (IBM SPSS Statistics, version 29.0.2.0, USA). For the primary variables derived from the secondary PCA analysis, an unpaired t-test was conducted to quantitatively compare the mean differences between each MRI FF group. Additionally, Pearson correlation analysis was performed to confirm the correlation between ultrasound-based biomarkers and MRI-FF values. This statistical approach served as the basis for evaluating how strongly the candidate variables derived from ultrasound imaging were associated with actual MRI-based fat quantification.

2.5. Machine Learning Prediction Model Development Procedure

In this study, data partitioning and preprocessing were performed as the foundational step for constructing a machine learning prediction model using the Matlab (MathWorks, Natick, MA, USA) program. During the data preprocessing stage, outliers and inconsistent data that could impair the model's predictive accuracy were strictly excluded. First, even if a particular variable was selected as a key variable in arbitrary tests, it was excluded if it exhibited low fit or inconsistent trends in the MATLAB-based linear regression analysis. This is because a high VIP Score for a variable does not necessarily guarantee a positive contribution to the prediction model; evaluating the model's actual applicability through regression analysis fit validation is essential. Second, measurements

 doi:10.20944/preprints202603.1260.v1

significantly affected by noise or show marked heterogeneity compared to other subjects' distributions were also excluded from analysis due to the nature of the subjects' imaging characteristics. These measures prevent the prediction model from overfitting due to distorted data or experiencing reduced generalization performance. Following this preprocessing, data from two subjects were excluded. Ultimately, the data from all 27 subjects were randomly split: data from 21 subjects were used for model training (training set), and data from the remaining 6 subjects were used for validation (validation set). Based on the data from these 21 subjects, those who underwent this systematic data preprocessing procedure, linear regression analysis and machine learning prediction model development were performed. This systematic data partitioning and preprocessing process is an essential step to enhance model stability and reliability and to develop clinically applicable quantitative ultrasound-based prediction models.

In this study, linear regression analysis was performed to predict MRI-based FF using candidate variables derived from ultrasound images. The analysis was conducted using Matlab software, and the entire procedure proceeded as follows. First, ultrasound indicators (independent variables, predictors) and MRI-FF values (dependent variable, response) were separated and organized as input data for constructing the regression model. Independent variables included slope, attenuation coefficient (alpha), R^2, and their composite/ratio variables obtained from the liver, spleen, and kidneys. The dependent variable was set as the MRI-FF value measured using the Dixon technique. Second, a linear regression model was fitted using the fitlm function in Matlab. In this process, the model was expressed as $Y = \beta_0 + \beta_1 X_1 + \beta_2 X_2 + \ldots + \beta nXn + \varepsilon$. Each coefficient ($\beta i$) was determined using the least squares method **[27]**. Third, the fitted regression model calculated metrics such as the coefficient of determination (R^2), p-value, and root mean square error (RMSE) to evaluate predictive performance. This allowed verification of each variable's explanatory power and the model's overall fit. Finally, cross-validation was performed to ensure model stability. To achieve this, the entire dataset was divided into a fixed number of folds, and training and validation were repeated by splitting data into folds. This minimized the risk of overfitting, where the model becomes overly dependent on a specific group of subjects. into folds, and by repeatedly performing training and validation, the risk of overfitting, which relies excessively on a specific group of subjects, was minimized. Through this procedure, a Matlab-based linear regression prediction model was constructed. This model was subsequently used in a complementary manner alongside nonlinear machine learning techniques in later stages.

3. Results

3.1. PCA and Derivation of Key Variables

In this study, PCA was performed to identify the correlation structure among quantitative variables derived from ultrasound images and to identify key variables contributing to the prediction of fatty liver. The initial PCA analysis reduced the dimensionality of the data by including all ultrasound-based variables and evaluated the interdependence among variables. This process yielded VIP values indicating each variable's contribution. Subsequently, to more precisely evaluate the group separability and predictive power among the variables, Partial Least Squares Discriminant Analysis (PLS-DA) and Orthogonal Partial Least Squares Discriminant Analysis (OPLS-DA) were additionally performed.

OPLS-DA analysis was performed independently for each MRI-FF-based group (<5% vs ≥5%, <5% vs ≥7%, <5% vs ≥10%, <5% vs ≥15%). Each analysis yielded various visual outputs, including loading scatter plots, score scatter plots, S-plots, and VIP plots. The results showed that, as depicted in (Figure 5), the OPLS-DA score scatter plot revealed a certain level of intergroup separation across all group comparisons. Notably, this separation tendency became distinctly apparent as MRI FF increased. This indicates that ultrasound-based signal attenuation variables form consistent patterns according to the degree of intrahepatic fat accumulation.

 doi:10.20944/preprints202603.1260.v1

Furthermore, the VIP score analysis identified variables with VIP ≥ 1.0 as key contributors to fatty liver classification across each MRI-FF reference group (<5% vs ≥5%: 112 variables, <5% vs ≥7%: 105 variables, <5% vs ≥10%: 100 variables, <5% vs ≥15%: 114 variables). These variables were primarily related to slope and alpha (exponential attenuation coefficient) measurements in the liver, kidney, and spleen regions.

Subsequently, a secondary PCA and OPLS-DA reanalysis was performed based on the VIP ≥ 1.0 variables derived from the initial PCA and OPLS-DA analysis. The purpose of the secondary analysis was to validate the consistency and stability of the key variables identified in the initial analysis and to evaluate the MRI-FF reference group (<5%, The purpose was to evaluate classification performance according to the threshold levels (≥5%, ≥7%, ≥10%, ≥15%). The secondary PCA reanalysis revealed that, using a VIP ≥ 1.0 threshold, over 40 variables were still derived for each MRI-FF group. This raised concerns about compromising model simplicity (parsimony) and interpretability. Therefore, to enhance the stringency of variable selection, the VIP threshold was raised to 1.25. As a result, In the <5% vs ≥5% group, 8 core variables were selected; in the <5% vs ≥7% group, 4; in the <5% vs ≥10% group, 6; and in the <5% vs ≥15% group, 6 (Table 1). These variables consistently demonstrated high discriminative contribution across all MRI-FF threshold conditions. Notably, the 'Alpha liver/kidney' ratio variable and the 'Liver Alpha R^2 DR200' variable were commonly included, validating consistency.

Table 1. Among variables with VIP score ≥ 1.0, over 40 features consistently showed high importance across MRI-FF threshold groups. Final ultrasound biomarkers were selected with VIP score ≥ 1.25 for subsequent data analysis.

MRI FF	VIP SCORE 1.0≥	VIP SCORE 1.25≥
<5% vs ≥5%	Alpha kidney200/liver100 Alpha kidney150/liver100 Alpha liver100/kidney150 Alpha liver100/kidney200 Liver alpha R^2 DR100 Liver slope R^2 DR200 Liver slope R^2 DR100 Liver slope R^2 DR150 Liver alpha R^2 DR200 Alpha liver200/kidney150 Liver alpha DR100 Liver alpha R^2 DR150	Alpha kidney200/liver100 Alpha kidney150/liver100 Alpha liver100/kidney150 Alpha liver100/kidney200 Liver alpha R^2 DR100 Liver slope R^2 DR200 Liver slope R^2 DR100 Liver slope R^2 DR150
<5% vs ≥7%	Alpha kidney200/liver100 Alpha kidney150/liver100 Liver alpha R^2 DR150 Liver slope R^2 DR150 Alpha liver200/kidney150 Liver alpha R^2 DR100 Alpha liver200/kidney100 Liver slope DR150 Liver slope R^2 DR200 Alpha kidney200/liver150 Mean_ alpha _Liver Alpha liver150/kidney200	Alpha kidney200/liver100 Alpha kidney150/liver100 Liver alpha R^2 DR150 Liver slope R^2 DR150
<5% vs ≥10%	Liver slope R^2 DR200 Liver alpha R^2 DR200 Alpha liver200/kidney100 Alpha liver200/kidney150 Alpha liver150/kidney100	Liver slope R^2 DR200 Liver alpha R^2 DR200 Alpha liver200/kidney100 Alpha liver200/kidney150 Alpha liver150/kidney100

 doi:10.20944/preprints202603.1260.v1

	Liver slope R^2 DR150 Mean_ alpha _Liver Alpha kidney150/liver100 Liver alpha R^2 DR150 Liver alpha DR100 Alpha kidney200/liver100 Alpha liver150/kidney200 ⋮	Liver slope R^2 DR150
<5% vs ≥15%	Liver alpha R^2 DR200 Alpha liver100/kidney200 Alpha liver100/kidney150 Liver slope R^2 DR200 Liver alpha R^2 DR150 Liver slope R^2 DR150 Alpha liver200/kidney100 Alpha liver200/kidney150 Liver alpha R^2 DR100 Alpha liver150/kidney200 Mean_ alpha _Liver Alpha kidney200/liver100	Liver alpha R^2 DR200 Alpha liver100/kidney200 Alpha liver100/kidney150 Liver slope R^2 DR200 Liver alpha R^2 DR150 Liver slope R^2 DR150

Consequently, the key variables derived through stepwise PCA and OPLS-DA approaches statistically demonstrated a close correlation between ultrasound attenuation characteristics and MRI-FF, indicating their potential as core input variables for future machine learning-based fatty liver prediction models.

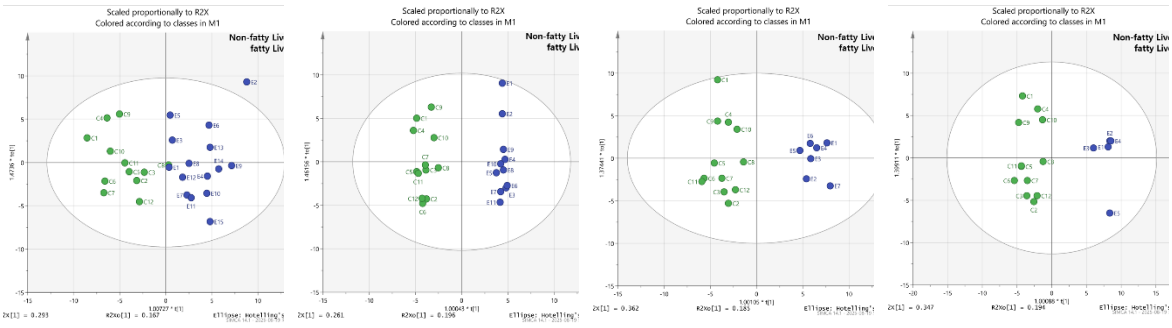

<5% vs ≥5% group **<5% vs ≥7% group** **<5% vs ≥10% group** **<5% vs ≥15% group**

Figure 5. Secondary PCA and OPLS-DA analyses conducted using variables with VIP ≥ 1.0 from the primary model. Purpose: to validate consistency and stability of key variables and assess classification performance by MRI-FF thresholds (<5%, ≥5%, ≥7%, ≥10%, ≥15%). OPLS-DA score plot demonstrated clear separation between non-fatty and fatty liver groups, indicating the quantitative relevance of ultrasound signal characteristics to hepatic steatosis severity.

3.2. Average Comparison of Ultrasound-Based Variables (Biomarkers)

3.2.1. Comparison of Mean Values for Key Variables Between MRI FF Groups

As shown in (Figure 6) A and B, comparison of the liver-to-kidney attenuation ratio (Alpha liver DR100/kidney DR150) based on MRI-FF criteria (<5% vs ≥5%, ≥15%) revealed significantly higher values in the fatty liver group compared to the non-fatty liver group. Particularly in the group with fat content ≥15%, the median value increased to approximately 3.5 or higher, showing a distinct difference compared to the non-fatty liver group (approximately 1.0).

 doi:10.20944/preprints202603.1260.v1

Furthermore, as shown in (Figure 6) C and D, comparing the determination coefficients (Liver alpha R^2 DR200) of the liver attenuation coefficient based on MRI-FF thresholds (<5% vs ≥10%, ≥15%) revealed significantly higher R^2 values in the fatty liver group compared to the non-fatty liver group. Specifically, as fat content increased to 15% or higher, the median value in the fatty liver group rose above 0.9, and the distribution range narrowed, indicating enhanced consistency in the signal attenuation pattern. In contrast, the non-fatty liver group maintained generally low R^2 values and exhibited a tendency toward greater variability. These results indicate that the attenuation coefficient model under DR200 conditions sensitively reflects the progression of fatty liver disease, and that the predictive accuracy of ultrasound signal attenuation improves as hepatic fat accumulation increases.

Finally, comparing the liver attenuation index (Liver slope R^2 DR200) according to MRI-based FF thresholds, as shown in (Figure 6) E, F, G, the R^2 values were significantly higher in the fatty liver groups (≥5%, ≥10%, ≥15%) than in the non-fatty liver group (<5%). Notably, as the threshold increased, the median value in the fatty liver group rose continuously, showing a clear tendency for the distributions between the two groups to separate distinctly.

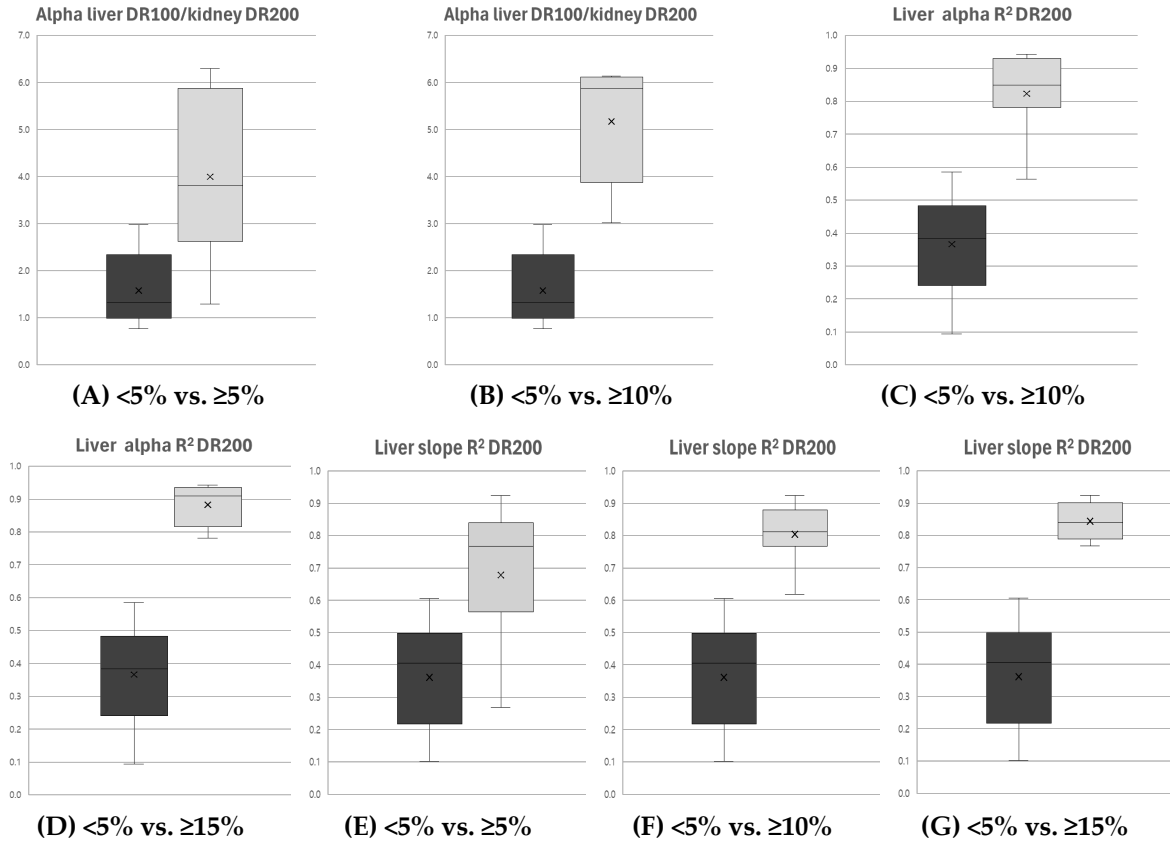

Figure 6. Ultrasound parameters, including Alpha liver/kidney ratio and Liver Alpha R^2 (DR200), showed significantly higher values in fatty liver groups (≥5%, ≥10%, ≥15%) than in non-fatty liver (<5%), indicating increased signal attenuation with hepatic fat accumulation. ■: Non-fatty Liver, ■: fatty Liver.

3.2.2. Summary of Correlation Analysis (Pearson's r) Results

As shown in Table 2, the correlation analysis between key biomarkers derived from MRI-FF and ultrasound imaging revealed that the variables Alpha liver 100/kidney 200, liver Alpha R2 DR200, and liver Slope R2 DR200 exhibited the highest correlations. The highest correlation coefficient was observed in Alpha liver 100/kidney 200 ($r=0.814$, $p<0.001$), confirming that the attenuation ratio between liver and kidney is the most sensitive indicator reflecting the degree of fat accumulation. This variable indicates that the attenuation of liver signals increases relatively sharply with increasing fat content, effectively describing quantitative changes in hepatic fat deposition.

 doi:10.20944/preprints202603.1260.v1

The second highest correlation was observed in liver Alpha R^2 DR200 (r=0.753, p<0.001), indicating that the attenuation curve fit (R^2) under the DR200 condition increases proportionally with fat content. This suggests that the ultrasound signal attenuation pattern with depth reflects the degree of fatty liver progression. The third highest variable, liver Slope R^2 DR200 (r=0.724, p<0.001), also showed a high positive correlation, indicating that changes in the slope of the signal intensity within the liver are consistently related to the degree of fat accumulation.

All three variables demonstrated high statistical significance and strong positive correlations, proving that the attenuation characteristics of ultrasound images can be reliably utilized as quantitative indicators of fatty liver.

Table 2. Pearson's correlation showed strong positive associations between MRI-FF and ultrasound biomarkers, with the highest correlation in Alpha liver 100/kidney 200 (r=0.814, p<0.001), followed by liver Alpha R^2 DR200 and liver Slope R^2 DR200, confirming their reliability as quantitative indicators of hepatic fat accumulation.

Biomarkers	Correlation coefficient value	p-value (two-tailed)
Alpha liver 100/kidney 200	.814**	<.001
Liver alpha R2 DR200	.753**	<.001
Liver slope R2 DR200	.724**	<.001
Alpha liver 100/kidney 150	.724**	<.001
Liver slope R2 DR150	.687**	<.001
Liver alpha R2 DR150	.681**	<.001
Liver alpha DR100	.680**	<.001
Alpha kidney200/liver100	-.651**	<.001
Alpha kidney150/liver100	-.644**	<.001
Liver alpha R2 DR100	.637**	<.001
Liver alpha DR150	.633**	<.001

3.3. Predictive Model Performance Evaluation)

This study constructed a machine learning prediction model to forecast MRI FF using ultrasound-based quantitative variables. The data from all 27 subjects were randomly divided, with 21 subjects' data used for model training and the remaining 6 subjects' data used for validation. For model training, key variables (VIP Score ≥ 1.25) selected through PCA were used as input values (VIP Score ≥ 1.25). To prevent overfitting (overfitting) of the data (5-fold cross-validation). After comparing multiple prediction models, the quadratic Support Vector Machine (SVM) model demonstrated the best performance.

The prediction performance evaluation revealed that the second-order SVM model had a root mean square error (RMSE) of 2.1997, and the correlation coefficient between the actual MRI-FF values and the predicted values was confirmed as r=0.82 (p<0.001). This indicates that the ultrasound-based variables reflect the degree of fatty liver measured by MRI with high accuracy. The trained model was converted into a function form within the MATLAB environment. As shown in (Table 3), the actual values and predicted values for the validation data (6 subjects) were compared using the formula yfit=trainedModel.predictFcn(T1~T6). The scatter plot visualizing the prediction results (Figure 7) showed that the actual and predicted values generally aligned around the ideal line, with the predicted values increasing linearly as fat content rose. Furthermore, graphs comparing the actual MRI-FF values and predicted values for individual subjects showed that most predicted values stably followed the trend of the actual values, supporting the model's reliability.

 doi:10.20944/preprints202603.1260.v1

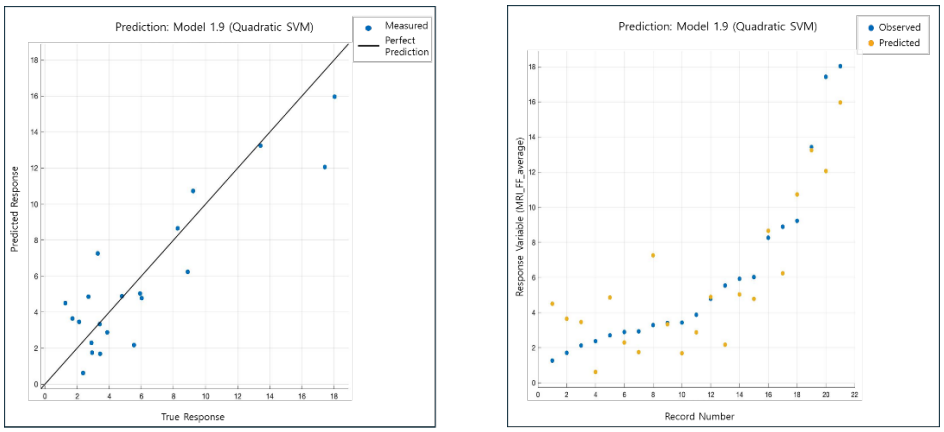

(A) Regression plot with ideal line **(B) Predicted vs. Actual plot**

Figure 7. As seen in Figure A generated by the MATLAB regression learner (Model 1.9, SVM), the actual values showed a similar trend along the ideal prediction line. Figure B confirms that the predicted FF increases linearly with the actual fat content. Most subject data consistently followed this trend, supporting the model's reliability.

These results demonstrate that quantitative variables such as the attenuation coefficient and reflectivity derived from ultrasound images can effectively estimate the degree of fatty liver disease through a machine learning-based quadratic SVM model. Notably, the SVM model is judged to significantly improve prediction accuracy compared to existing simple regression-based models by appropriately reflecting the complex nonlinear relationships between variables.

Table 3. The trained model was implemented in MATLAB as a prediction function (yfit = trainedModel.predictFcn(T1~T6)) to compare predicted and actual values in six validation subjects.

	Observed	Predicted
T1	16.42666667	18.7186
T2	12.155	16.5497
T3	6.996666667	11.1050
T4	7.781333333	9.3975
T5	26.39166667	24.5986
T6	27.37166667	34.1854

4. Discussion

This study aimed to develop a non-invasive predictive model for fatty liver disease using quantitative signal characteristics derived from ultrasound images, based on fat fraction (FF) quantified via the MRI DIXON technique. To achieve this, signal attenuation characteristics and reflectivity intensity of the liver, spleen, and kidneys were quantified from ultrasound images, and their correlation with MRI-FF was analyzed. Subsequently, variables with VIP scores ≥1.0 were selected via primary PCA analysis. Secondary PCA and OPLS-DA analyses verified variable contributions across various MRI-FF thresholds (<5%, ≥5%, ≥7%, ≥10%, ≥15%), thereby identifying candidate variables capable of stably contributing to the model without reliance on a single criterion. This stepwise approach aims to confirm whether physical variables, such as the signal attenuation characteristics obtained from ultrasound imaging, exhibit consistent trends with changes in fat content, and to optimize them as input variables for the predictive model. Ultimately, this study is significant in that it provides a fundamental basis for enabling MRI-level quantification of fatty liver disease based on quantitative analysis of ultrasound imaging.

 doi:10.20944/preprints202603.1260.v1

4.1. Predictive Model Performance Evaluation)

This study evaluated the correlation between quantitative variables extracted from ultrasound images and MRI FF, and based on this, constructed a machine learning model for predicting fatty liver. Analysis revealed that most ultrasound variables showed statistically significant correlations with MRI-FF. Specifically, the variables Alpha liver 100/kidney 200 (r=.814), liver Alpha R^2 DR200 (r =. 753), and liver Slope R^2 DR200 (r =. 724) exhibited the highest correlations. This indicates that the relative signal attenuation rate (alpha) between the liver and kidney, and the attenuation slope of liver parenchyma with depth, are sensitive to changes in fat content. In other words, as hepatic fat accumulation increases, the degree of ultrasound signal attenuation also increases. This characteristic showed a consistent trend with the fat fraction measured by MRI, holding significant clinical implications. The machine learning predictive analysis results also showed that the second-order SVM model demonstrated the highest predictive accuracy (RMSE=2.1997, r=0.82, $p<0.001$). The fact that the distributions of actual and predicted values approached a perfect prediction line and showed a linearly increasing pattern suggests that ultrasound-based quantitative variables can effectively estimate changes in MRI-FF. These results demonstrate that machine learning techniques, which reflect nonlinear characteristics, are more suitable for the quantitative prediction of fatty liver than existing simple regression-based approaches. This study demonstrated that signal attenuation coefficients and changes in reflectance intensity derived from ultrasound imaging can serve as quantitative indicators reflecting hepatic fat content. These findings show significant agreement with MRI-FF, suggesting the potential of ultrasound-based models as an alternative for non-invasive assessment of fatty liver disease.

4.2. Clinical Utility of Ultrasound-Based Variables

The ultrasound-based quantitative variables presented in this study demonstrate significant clinical utility as potential alternative indicators for non-invasively assessing the degree of fatty liver. Variables such as the signal attenuation ratio between the liver and kidney (alpha liver/kidney) and the attenuation slope within the hepatic parenchyma sensitively reflected changes in tissue acoustic properties associated with fat accumulation. These results indicate that ultrasound imaging can quantitatively assess the pathological changes in fatty liver disease by quantifying the acoustic properties of liver tissue, going beyond simple morphological evaluation [28]. MRI-PDFF is widely used as the standard for quantifying fatty liver disease, but its use in general clinical practice is constrained by limitations such as high cost, examination time, and accessibility [29]. In contrast, ultrasound offers high accessibility and facilitates repeated measurements. The quantitative variables derived in this study showed high correlation with MRI-FF, suggesting its potential to replace MRI or be utilized in the screening phase [30]. Specifically, alpha and slope indices possess the characteristic of being numerically quantifiable without relying on the examiner's subjective judgment, offering clinical advantages by ensuring inter-examiner reproducibility [31]. Furthermore, unlike existing blood tests or metabolic indicators such as BMI, ultrasound-based variables directly reflect physical changes in liver tissue. Therefore, they can be effectively utilized for early diagnosis of fatty liver disease or monitoring disease progression [32]. In the future, if these quantitative variables are combined with automated analysis systems or AI-based interpretation algorithms, they are highly likely to become non-invasive and efficient tools for the early prediction and follow-up observation of fatty liver disease.

4.3. Limitations and Complementary Aspects of Machine Learning Predictive Models

Recent advances in machine learning and deep learning technologies have dramatically improved the accuracy of medical image analysis[12,13]. Particularly in the field of ultrasound image analysis, algorithms such as Random Forest, XGBoost, and SVM have been successfully applied to the quantitative assessment of liver disease. Consequently, research is actively underway to transform examiner-dependent subjective readings into objective, quantitative indicators. Within this

 doi:10.20944/preprints202603.1260.v1

trend, this study attempted an approach to quantify the signal attenuation characteristics of ultrasound images and predict MRI-FF using a machine learning-based regression model. The machine learning-based fatty liver prediction model constructed in this study confirmed that MRI-FF can be predicted with high correlation using quantitative variables extracted from ultrasound images. However, several limitations exist. First, the analysis was based on a limited sample acquired from a single institution, limiting the model's generalizability. Signal intensity and attenuation coefficients can vary depending on imaging equipment, examination settings (DR 100-200), and subject characteristics, necessitating reproducibility verification using multi-center data or diverse ultrasound systems. Second, the machine learning model used in this study employed a relatively simple regression-based model (SVM), making it difficult to fully capture complex nonlinear relationships or subtle signal variations within tissues. In particular, the heterogeneity of intrahepatic fat distribution or the noise characteristics of ultrasound images can affect the model's predictive accuracy. Future work should apply deep learning-based regression models or ensemble learning to more accurately capture nonlinear signal characteristics. Third, while MRI-PDFF was used as a reference indicator in this study, liver biopsy is considered the definitive reference standard in actual clinical practice. Therefore, considering the potential discrepancy between MRI-PDFF and biopsy, the model's performance should be interpreted in terms of relative predictive capability rather than absolute accuracy. Fourth, the manual ROI setting in ultrasound images is another limitation. To minimize inter-observer variability, future studies should apply automated ROI detection and signal analysis algorithms to enhance consistency and objectivity. In summary, while the machine learning prediction model in this study demonstrated the potential for ultrasound-based quantitative assessment of fatty liver, future tasks include expanding its clinical reliability and applicability through securing more diverse data, refining the model, and introducing automated image analysis processes.

5. Conclusions

In this study, we developed a machine learning model to predict fatty liver using quantitative signal variables extracted from ultrasound images based on MRI fat fraction. Analysis revealed that key variables, such as the signal attenuation ratio between liver and kidney (Alpha liver 100/kidney 200) and the attenuation slope of hepatic parenchyma (Slope R^2 DR200), showed high correlation with MRI-FF. The quadratic SVM model demonstrated the highest predictive performance (RMSE 2.1997, $r=0.82$, $p<0.001$). These results indicate that ultrasound-based signal attenuation characteristics can quantitatively reflect hepatic fat accumulation, suggesting their potential as an objective indicator to replace existing subjective ultrasound assessments. Furthermore, ultrasound offers high accessibility and cost-effectiveness, resulting in lower patient burden and easier repeat measurements compared to MRI or CT, thereby demonstrating significant clinical utility. Therefore, the ultrasound-based prediction model proposed in this study is expected to serve as a non-invasive and practical alternative for the early diagnosis and follow-up of fatty liver disease in the future.

Author Contributions: Conceptualization, K.-S.C. and Y.-S.M.; methodology, K.-S.C.; software, K.-S.C.; validation, K.-S.C. and Y.-S.M.; formal analysis, K.-S.C.; investigation, K.-S.C.; resources, Y.-S.M.; data curation, K.-S.C.; writing—original draft preparation, K.-S.C.; writing—review and editing, K.-S.C. and Y.-S.M.; visualization, K.-S.C.; supervision, Y.-S.M.; project administration, Y.-S.M.; funding acquisition, Y.-S.M. All authors have read and agreed to the published version of the manuscript.

Funding: This research was supported by the Regional Innovation System & Education (RISE) program through the Jeonbuk RISE Center, funded by the Ministry of Education (MOE) and the Jeonbuk State, Republic of Korea (2025-RISE-13-JJU).

Institutional Review Board Statement: The study was conducted in accordance with the Declaration of Helsinki, and approved by the Institutional Review Board of Jeonju University (protocol code jjIRB-250529-HR-2023-1012 and date of approval: 29 May 2025).

 doi:10.20944/preprints202603.1260.v1

Informed Consent Statement: Informed consent was obtained from all subjects involved in the study. Written informed consent has been obtained from the patients to publish this paper.:

Data Availability Statement: The data presented in this study are available on request from the corresponding author due to privacy and ethical restrictions.

Acknowledgments: The authors would like to thank the Department of Radiologic Science at Jeonju University for providing the ultrasound diagnostic system (Samsung Medison H60) used in this study. We also express our sincere gratitude to Bon-yeol Ku from the Department of Radiology at Jeonju Vision University for his expert assistance with the ultrasound examinations. Additionally, during the preparation of this manuscript, the authors used Gemini (Google) for the purposes of English language editing and technical formatting. The authors have reviewed and edited the output and take full responsibility for the content of this publication.

Conflicts of Interest: The authors declare no conflicts of interest.

Abbreviations

The following abbreviations are used in this manuscript:

MRI	Magnetic Resonance Imaging
MRI-FF	MRI DIXON-based Fat Fraction
MRI-PDFF	MRI Proton Density Fat Fraction
FF	Fat Fraction
BMI	Body Mass Index
CT	Computed Tomography
DR	Dynamic Range
TGC	Time Gain Compensation
ROI	Region of Interest
PCA	Principal Component Analysis
PLS-DA	Partial Least Squares Discriminant Analysis
OPLS-DA	Orthogonal Partial Least Squares Discriminant Analysis
VIP	Variable Importance in Projection
SVM	Support Vector Machine
RMSE	Root Mean Square Error
R^2	Coefficient of Determination
SD	Standard Deviation
TR	Repetition Time
TE	Echo Time
FOV	Field of View
IP	In-phase
OP	Out-of-phase
NASH	Non-Alcoholic Steatohepatitis
AI	Artificial Intelligence
IRB	Institutional Review Board
USA	United States of America

References

1. Chalasani, N.; Younossi, Z.; Lavine, J.E.; Diehl, A.M.; Brunt, E.M.; Cusi, K.; Charlton, M.; Sanyal, A.J. The diagnosis and management of non-alcoholic fatty liver disease: practice guideline by the American Association for the Study of Liver Diseases, American College of Gastroenterology, and the American Gastroenterological Association. *Hepatology* **2012**, *55*, 2005–2023.
2. Kitade, H.; Chen, G.; Ni, Y.; Ota, T. Nonalcoholic fatty liver disease and insulin resistance: new insights and potential new treatments. *Nutrients* **2017**, *9*, 387.
3. Fon Tacer, K.; Rozman, D. Nonalcoholic Fatty liver disease: focus on lipoprotein and lipid deregulation. *Journal of lipids* **2011**, *2011*, 783976.

 doi:10.20944/preprints202603.1260.v1

4. Reeder, S.B.; Cruite, I.; Hamilton, G.; Sirlin, C.B. Quantitative assessment of liver fat with magnetic resonance imaging and spectroscopy. *Journal of magnetic resonance imaging* **2011**, *34*, 729–749.
5. Lee, S.S.; Park, S.H. Radiologic evaluation of nonalcoholic fatty liver disease. *World journal of gastroenterology: WJG* **2014**, *20*, 7392.
6. Hernaez, R.; Lazo, M.; Bonekamp, S.; Kamel, I.; Brancati, F.L.; Guallar, E.; Clark, J.M. Diagnostic accuracy and reliability of ultrasonography for the detection of fatty liver: a meta-analysis. *Hepatology* **2011**, *54*, 1082–1090.
7. Strauss, S.; Gavish, E.; Gottlieb, P.; Katsnelson, L. Interobserver and intraobserver variability in the sonographic assessment of fatty liver. *Am J Roentgenol* **2007**, *189*, W320–W323.
8. Strauss, S.; Gavish, E.; Gottlieb, P.; Katsnelson, L. Interobserver and intraobserver variability in the sonographic assessment of fatty liver. *Am J Roentgenol* **2007**, *189*, W320–W323.
9. Yajima, Y.; Ohta, K.; NARUI, T.; ABE, R.; SUZUKI, H.; OHTSUKI, M. Ultrasonographical diagnosis of fatty liver: significance of the liver-kidney contrast. *Tohoku J Exp Med* **1983**, *139*, 43–50.
10. Taylor, K.J.; Riely, C.A.; Hammers, L.; Flax, S.; Weltin, G.; Garcia-Tsao, G.; Conn, H.O.; Kuc, R.; Barwick, K.W. Quantitative US attenuation in normal liver and in patients with diffuse liver disease: importance of fat. *Radiology* **1986**, *160*, 65–71.
11. Zhang, Y.N.; Fowler, K.J.; Hamilton, G.; Cui, J.Y.; Sy, E.Z.; Balanay, M.; Hooker, J.C.; Szeverenyi, N.; Sirlin, C.B. Liver fat imaging—a clinical overview of ultrasound, CT, and MR imaging. *Br J Radiol* **2018**, *91*, 20170959.
12. Andre, M.P.; Han, A.; Heba, E.; Hooker, J.; Loomba, R.; Sirlin, C.B.; Erdman, J.W.; O'Brien, W.D. Accurate diagnosis of nonalcoholic fatty liver disease in human participants via quantitative ultrasound, 2014 IEEE International Ultrasonics Symposium, IEEE: 2014; , pp. 2375–2377.
13. Taylor, K.J.; Riely, C.A.; Hammers, L.; Flax, S.; Weltin, G.; Garcia-Tsao, G.; Conn, H.O.; Kuc, R.; Barwick, K.W. Quantitative US attenuation in normal liver and in patients with diffuse liver disease: importance of fat. *Radiology* **1986**, *160*, 65–71.
14. Valckx, F.; Thijssen, J.M.; Van Geemen, A.J.; Rotteveel, J.J.; Mullaart, R. Calibrated parametric medical ultrasound imaging. *Ultrason Imaging* **2000**, *22*, 57–72.
15. Tang, M.; Luo, F.; Liu, D. Automatic time gain compensation in ultrasound imaging system, 2009 3rd International Conference on Bioinformatics and Biomedical Engineering, IEEE: 2009; , pp. 1–4.
16. Ivosev, G.; Burton, L.; Bonner, R. Dimensionality reduction and visualization in principal component analysis. *Anal Chem* **2008**, *80*, 4933–4944.
17. Abdi, H.; Williams, L.J. Principal component analysis. *Wiley interdisciplinary reviews: computational statistics* **2010**, *2*, 433–459.
18. Kurita, T. Principal component analysis (PCA). In *Computer vision: a reference guide*Springer: 2021; pp. 1013–1016.
19. Zhang, Z.; Castelló, A. Principal components analysis in clinical studies. *Annals of translational medicine* **2017**, *5*, 351.
20. Raptis, D.A.; Fischer, M.A.; Graf, R.; Nanz, D.; Weber, A.; Moritz, W.; Tian, Y.; Oberkofler, C.E.; Clavien, P. MRI: the new reference standard in quantifying hepatic steatosis? *Gut* **2012**, *61*, 117–127.
21. Gupta, A.; Dixit, R.; Prakash, A. Non-invasive hepatic fat quantification: Can multi-echo Dixon help? *Radiologia Brasileira* **2024**, *57*, e20230125.
22. Noh, H.; Song, X.; Heo, S.H.; Kim, J.W.; Shin, S.S.; Ahn, K.Y.; Jeong, Y.Y.; Kang, H. Comparative study of ultrasonography, computed tomography, magnetic resonance imaging, and magnetic resonance spectroscopy for the diagnosis of fatty liver in a rat model. *Journal of the Korean Society of Radiology* **2017**, *76*, 14–24.
23. Tang, A.N.; Tan, J.; Sun, M.; Hamilton, G.; Bydder, M.; Wolfson, T.; Gamst, A.C.; Middleton, M.; Brunt, E.M.; Loomba, R. Nonalcoholic fatty liver disease: MR imaging of liver proton density fat fraction to assess hepatic steatosis. *Radiology* **2013**, *267*, 422–431.
24. Sirlin, C.B. Noninvasive imaging biomarkers for steatosis assessment. *Liver Transplantation* **2009**, *15*, 1389–1391.

 doi:10.20944/preprints202603.1260.v1

25. Lee, D.H.; Lee, J.Y.; Park, M.S.; Han, J.K. Non-invasive monitoring of hepatic steatosis via acoustic structure quantification of ultrasonography with MR spectroscopy as the reference standard. *Ultrasonography* **2020**, *39*, 70–78.
26. Tang, A.N.; Tan, J.; Sun, M.; Hamilton, G.; Bydder, M.; Wolfson, T.; Gamst, A.C.; Middleton, M.; Brunt, E.M.; Loomba, R. Nonalcoholic fatty liver disease: MR imaging of liver proton density fat fraction to assess hepatic steatosis. *Radiology* **2013**, *267*, 422–431.
27. Boglárka, Z.; Zsombor, Z.; Rónaszéki, A.D.; Egresi, A.; Stollmayer, R.; Himsel, M.; Bérczi, V.; Kalina, I.; Werling, K.; Győri, G. Construction of a Compound Model to Enhance the Accuracy of Hepatic Fat Fraction Estimation with Quantitative Ultrasound. *Diagnostics* **2025**, *15*, 203.
28. Ferraioli, G.; Wong, V.W.; Castera, L.; Berzigotti, A.; Sporea, I.; Dietrich, C.F.; Choi, B.I.; Wilson, S.R.; Kudo, M.; Barr, R.G. Liver ultrasound elastography: an update to the world federation for ultrasound in medicine and biology guidelines and recommendations. *Ultrasound Med Biol* **2018**, *44*, 2419–2440.
29. Castera, L.; Friedrich-Rust, M.; Loomba, R. Noninvasive assessment of liver disease in patients with nonalcoholic fatty liver disease. *Gastroenterology* **2019**, *156*, 1264–1281. e4.
30. Ferraioli, G.; Monteiro, L.B.S. Ultrasound-based techniques for the diagnosis of liver steatosis. *World journal of gastroenterology* **2019**, *25*, 6053.
31. Dag, N.; Igci, G.; Yagin, F.H.; Hanci, M.S.; Kutlu, R. Interobserver Reproducibility of Ultrasound Attenuation Imaging Technology in Liver Fat Quantification. *Journal of Clinical Ultrasound* **2025**, *53*, 405–412.
32. Yin, H.; Fan, Y.; Yu, J.; Xiong, B.; Zhou, B.; Sun, Y.; Wang, L.; Zhu, Y.; Xu, H. Quantitative US fat fraction for noninvasive assessment of hepatic steatosis in suspected metabolic-associated fatty liver disease. *Insights Into Imaging* **2024**, *15*, 159.